HHS Public Access

Author manuscript

Circulation. Author manuscript; available in PMC 2020 September 17.

Published in final edited form as:

Circulation. 2019 September 17; 140(12): 1015–1030. doi:10.1161/CIRCULATIONAHA.119.039710.

Disruption of Ca^{2+}_i homeostasis and Cx43 hemichannel function in the right ventricle precedes overt arrhythmogenic cardiomyopathy in PKP2-deficient mice

Joon-Chul Kim, PhD[1], **Marta Pérez-Hernández, PhD**[1], **Francisco J Alvarado, PhD**[2], **Svetlana R Maurya, PhD**[3], **Jerome Montnach, PhD**[4], **Yandong Yin, PhD**[5], **Mingliang Zhang, PhD**[1], **Xianming Lin, PhD**[1], **Carolina Vasquez, PhD**[1], **Adriana Heguy, PhD**[6], **Feng-Xia Liang, PhD**[7], **Sun-Hee Woo, PhD**[8], **Gregory E Morely, PhD**[1], **Eli Rothenberg, PhD**[5], **Alicia Lundby, PhD**[3,9], **Hector H Valdivia, MD, PhD**[2], **Marina Cerrone, MD**[1,*], **Mario Delmar, MD, PhD**[1,*]

[1]The Leon H Charney Division of Cardiology. New York University School of Medicine. New York NY.

[2]Department of Medicine and Cardiovascular Research Center, University of Wisconsin-Madison School of Medicine and Public Health. Madison WI.

[3]Department of Biomedical Sciences, Faculty of Health and Medical Sciences, University of Copenhagen.

[4]Institut du Thorax, Nouvelle Universite a Nantes. INSERM. Nantes Cedex 1, France.

[5]Department of Pharmacology and Biochemistry. New York University School of Medicine. New York NY.

[6]Department of Pathology and Genome Technology Center. New York University School of Medicine. New York NY.

[7]Microscopy laboratory, Division of Advanced Research Technologies. New York University School of Medicine. New York NY.

[8]Laboratory of Physiology, College of Pharmacy, Chungam National University, Daejeon, South Korea.

[9]NNF Center for Protein Research, Faculty of Health and Medical Sciences, University of Copenhagen

Abstract

Background—Plakophilin-2 (PKP2) is classically defined as a desmosomal protein. Mutations in PKP2 associate with most cases of gene-positive arrhythmogenic right ventricular cardiomyopathy (ARVC). A better understanding of PKP2 cardiac biology can help elucidate the

*co-corresponding authors, Address correspondence to: Mario Delmar MD PhD, The Leon H Charney Division of Cardiology, New York University School of Medicine, 435 East 30th Street. NSB 707, New York NY 10016, Phone number (212)263-9492, Mario.delmar@nyumc.org, Marina Cerrone, MD, The Leon H Charney Division of Cardiology, New York University School of Medicine, 435 East 30th Street. NSB 723H, New York NY 10016, Phone number: 212-263-9136, marina.cerrone@nyumc.org.

DISCLOSURE

None.

mechanisms underlying arrhythmic and cardiomyopathic events consequent to PKP2 deficiency. Here, we sought to capture early molecular/cellular events that can act as nascent arrhythmic/cardiomyopathic substrates.

Methods—We used multiple imaging, biochemical and high-resolution mass spectrometry methods to study functional/structural properties of cells/tissues derived from cardiomyocyte-specific, tamoxifen-activated, PKP2 knockout mice ("PKP2cKO") 14 days post-tamoxifen (post-TAM) injection, a time point preceding overt electrical or structural phenotypes. Myocytes from right or left ventricular free wall were studied separately.

Results—Most properties of PKP2cKO left ventricular (PKP2cKO-LV) myocytes were not different from control; in contrast, PKP2cKO right ventricular (PKP2cKO-RV) myocytes showed increased amplitude and duration of Ca^{2+} transients, increased [Ca^{2+}] in the cytoplasm and sarcoplasmic reticulum (SR), increased frequency of spontaneous Ca^{2+} release events (sparks) even at comparable SR load, and dynamic Ca^{2+} accumulation in mitochondria. We also observed early- and delayed-after transients in RV myocytes and heightened susceptibility to arrhythmias in Langendorff-perfused hearts. In addition, RyR2 in PKP2cKO-RV cells presented enhanced Ca^{2+} sensitivity and preferential phosphorylation in a domain known to modulate Ca^{2+} gating. RNAseq at 14 days post-TAM showed no relevant difference in transcript abundance between RV and LV, neither in control nor in PKP2cKO cells. Instead, we found an RV-predominant increase in membrane permeability that can permit Ca^{2+} entry into the cell. Cx43 ablation mitigated the membrane permeability increase, accumulation of cytoplasmic Ca^{2+}, increased frequency of sparks and early stages of RV dysfunction. Cx43 hemichannel block with GAP19 normalized $[Ca^{2+}]_i$ homeostasis. Similarly, PKC inhibition normalized spark frequency at comparable SR load levels.

Conclusions—Loss of PKP2 creates an RV-predominant arrhythmogenic substrate (Ca^{2+} dysregulation) that precedes the cardiomyopathy; this is, at least in part, mediated by a Cx43-dependent membrane conduit and repressed by PKC inhibitors. Given that asymmetric Ca^{2+} dysregulation precedes the cardiomyopathic stage, we speculate that abnormal Ca^{2+} handling in RV myocytes can be a trigger for gross structural changes observed at a later stage.

Keywords

ARVC; right ventricle; PKP2: sudden death; calcium homeostasis; connexin43 hemichannel

INTRODUCTION

Plakophilin-2 (PKP2) is classically defined as a protein of the desmosome, an intercellular adhesion structure. Recent studies demonstrated that in addition to cell-cell adhesion, PKP2 translates information initiated at the site of cell-cell contact into intracellular signals that maintain structural and electrical homeostasis[1–4]. Mutations in *PKP2* associate with most cases of gene-positive arrhythmogenic right ventricular cardiomyopathy (ARVC), a pleiotropic disease that can manifest as mainly electrical, structural or both depending on stage progression[5]. As such, while ARVC is best recognized as a cardiomyopathy of right ventricular predominance, catecholaminergic sudden cardiac arrest is common during the

subclinical (or “concealed”) phase of the disease[5–7]. The molecular/cellular mechanisms responsible for these arrhythmias remain unclear.

To study the role of cardiomyocyte PKP2 expression in cardiac function we utilized a cardiomyocyte-specific, tamoxifen (TAM)-activated, PKP2 knockout murine line (*Pkp2* fl/fl, αMyHC-Cre-ER(T2), dubbed “PKP2cKO”). We previously reported that adult PKP2cKO mice present, in a compressed time line, aspects of the history of human ARVC[3]. Following TAM injection these hearts progress from a normal state, to an arrhythmogenic cardiomyopathy of right ventricular (RV) predominance and eventually biventricular dilated cardiomyopathy and end-stage failure. The time course of this process is reproducible, allowing us to study the molecular environment at a given phenotype stage.

The earliest functional event detectable in PKP2cKO mice is an increase in RV area (measured by echocardiography 14 days post-TAM) and a high propensity to Isoproterenol-induced lethal ventricular arrhythmias at day 16 post-TAM. These events occur in the setting of preserved left ventricular ejection fraction (LVEF) and in the absence of increased collagen abundance or other changes in ventricular wall morphology (i.e., during a “concealed stage” preceding “overt” arrhythmogenic cardiomyopathy[3, 5, 7]). Thus, for this study, we focused on mice 14 days post-TAM, so as to capture early molecular/cellular events that can act as nascent arrhythmia substrates. Knowing that PKP2 deficiency first leads to a structural phenotype of RV predominance[3] we separately studied myocytes from right versus left free ventricular walls. We focused on possible changes in intracellular Ca^{2+} cycling, given previous evidence showing PKP2-mediated transcriptional regulation of intracellular Ca^{2+} homeostasis in the cardiomyopathic stage[3]. Overall, we found that loss of PKP2 creates not only an RV-predominant cardiomyopathy but also an RV-predominant arrhythmogenic substrate that precedes the cardiomyopathy and that is, at least in part, dependent on Cx43 expression/function. We speculate that disrupted $[Ca^{2+}]_i$ homeostasis in RV myocytes can be one of the triggers for gross structural changes in the RV at a later stage.

METHODS

We utilized a commercially available C57BL/6 *CX43*^{flox} mice line (Jackson Laboratory B6.129S7-Gja1$^{tm1.1Dlg}$/J, stock number 008039; loxP sites flank exon 2 of *Gja1*; first reported by Liao et al[8] and extensively studied in various systems; see e.g.[9]), crossed with PKP2flox/flox/αMHC-Cre-ER(T2) to obtain (CX43flox/flox)/(PKP2flox/flox)/Cre+, and CX43flox/wt)/(PKP2flox/flox)/Cre+ mice. All procedures conformed to the Guide for Care and Use of Laboratory Animals of the National Institutes of Health and were approved by the NYU-IACUC committee. For cardiac-specific *Pkp2* and/or *Gja1* deletion, mice were intraperitoneally injected 4 consecutive days with TAM (0.1 mg/g body weight). Cre-negative flox-positive, TAM-injected littermates were used as controls. Separate controls with TAM-injected, Cre-positive PKP2flox/wt showed no effects on life expectance or LVEF in a prolonged time window (Figure I, online-only data supplement), consistent with previous observations[10]. Both genders were included and all animals were between 3 and 6 months-old. Further details in online-only Data Supplement.

Procedures used for RNAseq, cardiomyocyte dissociation, Ca^{2+} imaging, Western blots, single-molecule localization microscopy (SMLM), serial block-face scanning electron microscopy (SB-SEM), [^{3}H]Ryanodine binding assays, mass spectrometry, echocardiography, patch clamp and voltage-sensitive optical mapping followed those previously published and are detailed in the online-only Data Supplement.

For evaluation of membrane permeability in whole hearts, two fluorescent dyes, Lucifer Yellow (LY) and Rhodamine Dextran (RD), were used to quantify the entry of a small molecular weight dye into Langendorff-perfused hearts. Hearts were washed, fixed, epicardium was manually removed, free walls separated and placed epicardial face down for observation by fluorescence confocal microscopy. Imaging was performed at several randomly chosen sites in each tissue sample. Details in online-only Data Supplement.

Statistical analysis

Numerical results are given as means ± standard error of the mean (S.E.M.). Two-way repeated measures ANOVA followed by Bonferroni post-hoc test was used for most data sets. In specific cases (noted in the respective figure legends), paired or unpaired Student's t-test, one-way repeated measures ANOVA-Bonferroni or Chi-square test was used. Analysis was done using OriginPro 8, Origin 2018b, SPSS 25 and SigmaPlot 13 packages. Differences were considered to be significant at $p<0.05$. Hierarchical analysis was carried out as indicated in Figure legends. Of note, this resource first detects adequacy of hierarchical analysis vis a vis other methods; analysis was carried out accordingly for each data set.

Data Availability

The data that support the findings of this study are presented in the manuscript and online supplementary files, and additional information can be made available from the corresponding author upon reasonable request.

RESULTS

Ca^{2+} transients in cardiomyocytes from PKP2cKO hearts

We determined amplitude and time course of Ca^{2+} transients of RV and LV myocytes from control and PKP2cKO hearts using conventional pacing protocols (e.g[3]). Figures 1A and 1B show time-space plots and time course of Ca^{2+} transients, respectively, recorded by line-scanning confocal microscopy in cells loaded with Fluo-4 and field-stimulated at 1 Hz. Data from LV and RV (control and PKP2cKO) are shown to the left and right of the panels, respectively. Compiled data are shown in panels C-E. In this and subsequent figures, black and red bars represent data from control and PKP2cKO, respectively. The data show that transient amplitude was larger in PKP2cKO-RV myocytes when compared to either control, or PKP2cKO-LV myocytes (panel C). Loss of PKP2 also led to prolongation of Ca^{2+} transient decay, which was statistically significant in RV myocytes (panel D). No difference was apparent in time-to-peak in either group (panel E). Of note, incidence of early and delayed after-transients and of spontaneous Ca^{2+} waves was significantly higher in

PKP2cKO-RV myocytes when compared to PKP2cKO-LV myocytes or control (see Figure II, online-only Data Supplement).

Functional changes were accompanied by changes in protein abundance. Western blots showed reduced expression of PKP2 in both ventricles (Figure III, online-only Data Supplement). In contrast, RyR2 abundance was higher in LV than RV of controls (Fig.III, online-only Data Supplement), and of PKP2cKO mice, rendering significant RV-LV asymmetry. Reduced SERCA2a was also observed in PKP2cKO-RV when compared to PKP2cKO-LV (Fig.III, online-only Data Supplement). Patch clamp experiments at fixed [Ca^{2+}] detected no difference in peak NCX current density (Figure IV, online-only Data Supplement).

Increased spontaneous Ca^{2+} release in PKP2cKO RV myocytes

Figure 1F shows confocal line-scan images of Ca^{2+} sparks (arrows) from LV or RV intact cells of control or PKP2cKO mice 14 days post-TAM. Figures 1G–K show compiled results. Ca^{2+} sparks frequency was similar for control myocytes regardless of provenance (RV or LV) and also similar to PKP2cKO-LV myocytes. However, the frequency of Ca^{2+} sparks was significantly higher in PKP2cKO-RV myocytes (Figure 1G), though no difference in amplitude of events or full-width at half maximum (FWHM) was detected (Figure 1H–I). Ca^{2+} sparks from PKP2cKO myocytes showed longer durations (full duration at half maximum; FDHM; Figure 1J) and time-to-peak (Figure 1K). These results, together with those in Figure 1A–D, indicate that loss of PKP2 increases the propensity of Ryanodine Receptor 2 (RyR2) channels to release Ca^{2+} preferentially in the RV. We therefore investigated whether this RyR2 eagerness associated with one or more of the following: a) a change in the transcriptional program of the cells (as it occurs during the cardiomyopathic stage; see[3]), b) functional changes intrinsic to the RyR2 protein, and/or c) an increase in the amount of Ca^{2+} in the intracellular compartments.

RNAseq RV versus LV: no major transcriptional differences

We examined the differential transcriptome (RV versus LV) of normal and PKP2cKO hearts. (Complete datasets in Tables I and II, online-only Data Supplement.) Relative transcript abundance was determined from paired samples, by calculating the ratio RV/LV for each transcript in the same animal. Positive or negative Log_2FC values therefore indicated over-representation of the transcript in RV or in LV, respectively. Volcano plots of differential transcriptomes (control and PKP2cKO mice) are presented in Figure V of online-only Data Supplement. In controls, only 21 transcripts were differentially expressed with log2Fc values larger than +/−1.0 and FDR values <0.01. Similar results were obtained for the differential RV vs. LV free wall transcriptome of PKP2cKO hearts, where only nine transcripts were differentially expressed, and 4 of them were also differentially expressed in the controls. These results suggest that, as opposed to what occurs at the cardiomyopathic stage[3], our data cannot be explained by PKP2-dependent changes in transcript abundance of molecules directly involved in regulation of $Ca^{2+}{}_i$ homeostasis.

Structural and functional properties of RyR2 in PKP2cKO myocytes

We examined three aspects of RyR2: Its nanostructural organization into clusters, its sensitivity to Ca^{2+}, and its phosphorylation state.

RyR2 super-clusters in PKP2cKO myocytes—Recent studies show that when two small RyR2 clusters are at a distance of ≤100nm from each other, the probability for propagating Ca^{2+} release is increased ("super-clusters[11–13]). Data also show that a heterogeneous population of clusters (co-existence of super-clusters and large single clusters) can lead to increased susceptibility to calcium waves[14]. Figure 2A shows SMLM images of clusters of RyR2 from control or PKP2cKO adult ventricular myocytes 14 days post-TAM. In Figure 2B, areas in yellow boxes are enlarged and displayed in black and white to enhance contrast. All clusters were analyzed for size and proximity (see, e.g.[15]). RyR2 clusters were, on average, significantly smaller in PKP2cKO cells (Figure 2C). The subpopulation of clusters occupying an area ≤14,000 nm^2 (such as those in insets of Figure 2B) was subsequently analyzed to identify the fraction of clusters whose edges were within 100 nm from each other ("super-clusters;" see diagram in Figure 2D). Cumulative data (Figure 2D) show that the proportion of "super-clusters" was higher in PKP2cKO and that they co-existed with large clusters, forming a heterogenous population likely to provide a structural substrate for enhanced Ca^{2+} release[14]. Importantly, the frequency of super-clusters was similar in myocytes from RV versus LV of PKP2cKO mice. We then calculated the number of RyR2 units and their density utilizing Density-Based Spatial Clustering of Applications with Noise (DBSCAN; see online-only Data Supplement). The median number of RyR2 units per cluster (between 30 and 58 RyR2 units; Figures VI and VII, online-only Data Supplement) was within the range of what has been previously reported[11–13]. However, the density of RyR2 units within a cluster (number of RyR2 units per nm^2) was significantly larger in PKP2cKO cells when compared to control (Figure 2E), likely facilitating cross-activation of Ca^{2+} induced Ca^{2+} release. Yet, the absence of right-left asymmetry suggests that this difference is not, per se, a mechanism for preferential increased Ca^{2+} release in RV myocytes. As a next step, we examined the Ca^{2+} sensitivity and phosphorylation state of RyR2 channel proteins.

Reduced expression and enhanced Ca^{2+} sensitivity of RyR2 in PKP2cKO-RV myocytes—[^{3}H]Ryanodine binding assays were carried out from right and left ventricular tissue, harvested 14 days post-TAM, to determine Ca^{2+} sensitivity of RyR2 channels in PKP2cKO hearts versus controls. The plots in Figure 3A–B and the bar graph in Figure 3C show that, while samples collected from the PKP2cKO-LV showed a similar Ca^{2+} response as controls, samples from the RV of PKP2cKO mice showed a lower B_{max}, consistent with lower RyR2 expresion (Figure VIII, online-only Data Supplement). Normalization of [^{3}H]ryanodine binding to levels observed at the highest Ca^{2+} concentration (10 μM) revealed no difference between PKP2cKO-LV and control samples, but a left-shift (enhanced Ca^{2+} sensitivity; reduced EC_{50}) for PKP2cKO-RV hearts (Figure 3D–F).

Differential phosphorylation state of RyR2: phosphorylation of T2809 in the RV—In addition to Ca^{2+} sensitivity, SR Ca^{2+} release can be modulated by RyR2 phosphorylation (e.g.,[16–18]). Accordingly, we evaluated the phosphorylation state of RyR2

in RV and LV of four PKP2cKO mice 14 days post-TAM using high-resolution mass spectrometry[19] (also online-only Data Supplement). Our measurements covered 13 phosphorylation sites on RyR2, 11 of which were class 1 sites with high confidence in phosphorylation site localization (Figure 4A). Figure 4B presents a summary of intensity measurements of all RyR2 phosphopeptides across samples. Notice that amino acids S2807 and S2813, previously characterized as preferential substrates for PKA and CAMKII, respectively (and annotated as "S2808" and "S2814" in the old nomenclature), are detected as phosphorylated in all samples, irrespective of provenance. However, there was a clear distinction between phosphorylation states of residue T2809. All four PKP2cKO-RV samples showed high levels of T2809 phosphorylation, whereas phosphorylation on this residue was not detected in samples from PKP2cKO-LV. Figure 4C shows an MS/MS spectrum of T2809 phosphorylation measured in a PKP2cKO-RV sample underscoring the certainty in site localization to this residue. T2809, not previously characterized as substrate for kinase regulation of RyR2 and yet located in the same "phosphorylation hotspot" known to regulate RyR2 gating[20] is highly conserved across species. Samples from over 120,000 individuals deposited in gnomAD show no variance in T2809, suggesting biological relevance. According to NetPhos3.1 (www.cbs.dtu.dk/services/NetPhos/), the probability of T2809 to be a PKC substrate is estimated at 0.721 in the human sequence and 0.671 in the case of mouse (Figure IX, online-only Data Supplement[21, 22]). The bar graph in Figure 4D summarizes the results and shows that T2809 phosphorylation was also absent in 4 control hearts. Interestingly, S2810, another phospho-site not yet fully characterized and located within the same "hotspot," was phosphorylated exclusively in PKP2cKO samples, though to a similar level in RV and LV (Figure 4D).

Intracellular Ca^{2+} content

Increased SR load in PKP2cKO RV myocytes—In addition to properties intrinsic to RyR2, we examined whether enhanced Ca^{2+} sparks coincided with differences in abundance of stored Ca^{2+} in the intracellular space. The sarcoplasmic reticulum (SR) Ca^{2+} load of intact (non-permeabilized) myocytes was estimated from the amplitude of caffeine-induced Ca^{2+} transients, using a ratiometric dye method[23, 24]. As show in Figure 5A and 5B, SR Ca^{2+} content of PKP2cKO-RV myocytes was higher than in PKP2cKO-LV or in myocytes from controls (Figures 5B and 5C). Similar results were obtained from permeabilized myocytes using a method previously implemented in our laboratory[3] (Figure X, online-only Data Supplement).

Increased [Ca^{2+}] in the cytoplasmic and mitochondrial compartments—The SR was not the only intracellular compartment with increased Ca^{2+} load. Indeed, as shown in Figures 5D and 5E, cytoplasmic resting Ca^{2+} content was higher in PKP2cKO myocytes (also Figure X, online-only Data Supplement). Furthermore, using a Ca^{2+} indicator (Rhod-2) that enters the mitochondrial space in a temperature-dependent manner[25] (see also Figure XI, online-only Data Supplement), we unveiled a dynamic Ca^{2+} accumulation in mitochondria of isolated PKP2cKO-RV myocytes after a brief period of pacing (one minute at 3 Hz; Figures 5F and 5G). Altogether, the results reveal increased [Ca^{2+}] in all three major compartments (SR, cytoplasmic and mitochondrial) in PKP2cKO-RV myocytes when compared to PKP2cKO-LV or control myocytes.

Spark frequency at comparable SR load; effect of PKC inhibition—The observations above raised the question of whether increased spark frequency in PKP2cKO-RV myocytes was consequent to increased SR load, enhanced RyR2 release of Ca^{2+}, or both. We therefore analyzed spark frequency at comparable levels of SR load using a procedure similar to that of Kim et al[26]. Control experiments showed that reducing $[Ca^{2+}]_o$ to 0.6 mM in PKP2cKO-RV myocytes yielded a comparable SR load to that obtained in PKP2cKO-LV myocytes at 1.8 mM $[Ca^{2+}]_o$ (see Fig. XII, online-only Data Supplement). Under those circumstances, spark frequency decreased, but remained higher than that observed in either control myocytes or in PKP2cKO-LV cells (Figure 6; blue bars). Further reduction of spark frequency was obtained when GF 109203X or Calphostin C, both inhibitors of PKC activity[26], were added to the external solution (blue bars with a + sign in Figure 6E). These results indicate that both increased SR load and enhanced RyR2 Ca^{2+} release contribute to heightened abundance of calcium sparks in PKP2cKO-RV myocytes, and that the latter is susceptible to inhibition by PKC antagonists.

Increased membrane permeability in PKP2cKO-RV myocytes: Role of Cx43

The results above led to the question of the source of excess intracellular Ca^{2+}. As one possibility, we examined whether increased membrane permeability would be a factor, and whether the permeable conduit would be dependent on Connexin43 (Cx43) expression. Considering that Cx43 internalizes after dissociation[27], we devised a protocol for analysis of Lucifer yellow (LY; mw 457) transfer in Langendorff-perfused whole heart preparations (see Methods). Figure 7A shows fluorescence confocal images of a control (left) and a PKP2cKO mouse heart 14 days post-TAM (middle). Images were collected from LV (top) and RV (bottom). Of note, Rhodamine Dextran (RD; mw ~10,000 Da) was also loaded and was not found in the intracellular space, confirming that LY did not enter cells through damaged sarcolemma (see Figure XIII, online-only Data Supplement). A quantitative analysis is shown in panel 7B (black and red bars). Notice the increased fluorescence apparent in PKP2cKO hearts, more prominently in the RV (black versus red bars in 7B).

Neither the abundance nor the subcellular localization of Cx43 were affected by loss of PKP2 expression at 14 days post-TAM (Fig. XIV, online-only Data Supplement). To define whether increased fluorescence was dependent on Cx43 function, we crossed PKP2cKO mice with a commercially available Cx43 fl/fl line (first described in[8]) to obtain, in response to TAM, a double PKP2-Cx43 knockout (refered to as PKP2-Cx43cKO). The mice developed normally and heart function prior to TAM was not different from control. As previously reported, life expectancy in Cx43-KO animals is limited, given their high likelihood of arrhythmic death[28–30]. Two out of 4 TAM-injected animals survived to day 14 post-TAM. As shown in Figure 7A (right column) and Figure 7B (blue bars), loss of Cx43 expression blunted the excess LY signal captured from either LV or RV. Interestingly, the increased membrane permeability was observed for both RV and LV PKP2cKO samples at a later time (21 days post-TAM; Figure XV, online-only Data Supplement) and in both cases, reduced Cx43 (PKP2cKO and Cx43 heterozygous; PKP2cKO/Cx43+/−) was sufficient to limit the increased membrane permeability to LY (green versus red bars in Figure XV, online-only Data Supplement). These results suggest that in the PKP2cKO there is a Cx43-

dependent mechanism in place that allows for small molecules to enter the cytoplasmic space.

Reduced Cx43 normalized diastolic $[Ca^{2+}]_i$ and spark frequency in PKP2cKO hearts

Based on the results in Figure 7A–B we tested whether elevated levels of diastolic Ca^{2+} and/or increased Ca^{2+} spark frequency in PKP2cKO-RV myocytes could be prevented by reducing Cx43 abundance. As shown in Figure 7C, cells obtained from PKP2cKO mice also heterozygous-null for cardiomyocyte Cx43 (PKP2cKO/Cx43+/−) showed a level of $[Ca^{2+}]_i$ that was not different from control. Spark frequency (at 1.8 mM $[Ca]_o$) was significantly reduced when compared to that obtained from PKP2cKO-RV cells, though remained higher than what was observed in control RV myocytes (Figure 7D).

To further ascertain the role of Cx43, we examined SR load, spark frequency and Ca^{2+} transient amplitude in PKP2cKO myocytes exposed to the Cx43 hemichannel inhibitor TAT-Gap 19 (GAP19;[31, 32] see also Figure XVI, online-only data supplement). As shown in Figure 8, this manipulation blunted the effect of PKP2 knockdown, reducing all parameters to levels that, for SR load, diastolic $[Ca^{2+}]$ and transient amplitude, were not significantly different from those observed in PKP2cKO-LV or control myocytes. As in the case of the PKP2cKO/Cx43+/− cells, spark frequency remained slightly higher in PKP2cKO-RV after GAP19, perhaps reflecting a direct effect of PKP2 knockdown on RyR2 function independent from increased Cx43-dependent calcium load.

Reduced Cx43 mitigated the increase in RV area in PKP2cKO hearts

The earliest functional event reported for PKP2cKO hearts was an increase in RV area at 14 days post-TAM.[3] As shown by the green bars in Figure XVII in online-only Data Supplement, a reduction in Cx43 gene dose mitigated the increase in RV area, which was significantly smaller in PKP2cKO/Cx43+/− when compared to PKP2cKO mice at 14 days post-TAM. This result further supports the notion of a role for Cx43 in the early stage pathophysiology that results from PKP2 loss of expression.

PKP2cKO and cellular/subcellular structure at 14 days post-TAM

We evaluated whether the events described above were associated with structural changes at the cellular/subcellular level. Measurements of cell size (length, width and area), membrane capacitance (as a surrogate for sarcolemal surface area) and sarcomere length were not different between the four groups (Control and PKP2cKO; RV and LV; Figure XVIII, online-only Data Supplement). Interestingly, SMLM of phosphoPKC localization (T368–641) at the cell end showed reduced cluster size and a tendency toward reduced density in PKP2cKO-RV when compared to control, and separation from the adhesive complex, marked by N-Cadherin localization (e.g.[33]; see Figure XIX, online-only Data Supplement). These data were in agreement with previous studies indicating dislodgment from PKC at the cell junction after loss of mechanical junction integrity[2]. Furthermore, consistent with the loss of a molecule of the adhesion complex (PKP2), ultrastructural analysis of intercalated disc of PKP2cKO RV tissue showed widening of the intercellular space when compared to an RV sample from a control mouse (Figure XX, online-only Data Supplement, and videos 1–2, online-only Data Supplement).

Enhanced susceptibility to arrhythmias in PKP2cKO hearts—The results presented above led us to examine the arrhythmia susceptibility of PKP2cKO hearts at 14 days post-TAM. As shown in Figure XXI in online-only Data Supplement, a rapid pace protocol in isoproterenol-exposed Langendorff-perfused hearts led to long runs of ventricular tachycardia in PKP2cKO animals. A similar protocol failed to induce arrhythmias in hearts from control littermates.

DISCUSSION

Previously, we showed that PKP2cKO mice develop an arrhythmogenic cardiomyopathy of RV predominance 21 days post-TAM injection[3]. To understand its cellular/molecular substrates, here we studied these mice at a time preceding the overt phenotype (i.e., 14 days –post-TAM) and looked for side-specific differences (RV vs. LV). Given our previous data[3], and given that the phenotype once apparent is both structural and electrical, we focused on a cellular function at the center of both excitability and contraction, namely, regulation of $[Ca^{2+}]_i$.

At 14 days post-TAM mice did not show cardiac fibrosis, cellular dimensions were similar to those in control, and LVEF was within normal limits. Transcriptome differences were minor and levels of PKP2 were drastically down in both ventricles. Yet, we detected important differences in $[Ca^{2+}]_i$ handling in PKP2cKO RV myocytes, while PKP2cKO LV myocytes remained similar to control. These differences were sensitive to Cx43 reduced expression or Cx43 hemichannel block, and coincided with a Cx43-dependent increase in membrane permeability of the RV, an RV-selective increase in $[Ca^{2+}]$ sensitivity of RyR2 and an RV-selective phosphorylation of RyR2-Thr2809, an amino acid within the “phosphorylation hotspot” of RyR2 long known to modulate channel gating. The eagerness of RyR2 to trigger Ca^{2+} sparks was tempered by exposing cells to PKC inhibitors. Based on previous knowledge regarding: a) the relation between $[Ca^{2+}]_i$ alterations and arrhythmia susceptibility, b) the importance of regional heterogeneity on arrhythmia generation, and c) the relation between $[Ca^{2+}]_i$ and cardiac remodeling[34, 35] we propose that $[Ca^{2+}]_i$ overload and RyR2 dysfunction play a central role in the generation of the electrical and RV-predominant structural phenotype in PKP2-deficient mice.

The Cx43-dependent increase in membrane permeability reported here can explain the excess $[Ca^{2+}]_i$. We speculate that PKP2 deficiency causes an excess of “orphan” Cx43 membrane hemichannels that can act as conduits for Ca^{2+} entry. Gap junction plaque formation is known to depend on proper intercellular adhesion[27]. It is also known that Cx43 hemichannels reside in the perimeter of the gap junctions (the perinexus)[36] and are capable, when undocked and in the membrane, to flicker with very low probability[37, 38]. Further supporting the relation between PKP2 expression and Cx43-dependent permeable conduits is a recent study showing that PKP2 deficiency can increase cell membrane permeability to ATP, an event prevented by silencing Cx43 expression[39]. We postulate that loss of PKP2 expression, perhaps via weakened intercellular adhesion consequent to loss of desmosomal integrity, causes an increased population of orphan, flickering Cx43 hemichannels that allow for excess entry of Ca^{2+} into the cell. It is worth noting that studies in cell culture systems and in human tissue from ARVC-affected patients have consistently reported that loss of

expression or mutations in PKP2 can alter the structure and function of gap junctions[40–42]. We did not detect changes in Cx43 abundance or in gap junction structure, suggesting that functional dysregulation of Cx43 hemichannel activity, coincident with nanostuctural changes in the intercalated disc, are among the earliest events following loss of PKP2 expression.

We found increased Ca^{2+} sparks frequency in PKP2cKO-RV myocytes. In addition to increased SR Ca^{2+} load and higher diastolic $[Ca^{2+}]_i$, this result may associate with increased sensitivity of RyR2 to Ca^{2+}, as well as a change in the phosphorylation state of RyR2-T2809. This residue is located near serine residues well studied as PKA and CAMKII substrates that, when phosphorylated, modify RyR2 gating behavior[20]. We do not know the kinase phosphorylating T2809; yet, sequence analysis, and data showing that PKC inhibitors reduced Ca^{2+} sparks frequency at comparable levels of SR load support the hypothesis of PKC involvement. Interestingly, previous work has shown that PKP2 is necessary to recruit and retain PKC at the desmosome, and that loss of desmosomal integrity releases PKC, freeing it to phosphorylate unintended targets[2]. Consistent with this notion, our SMLM data indicated reduced phospho-PKC cluster size and density at cell end, and increased phospho-PKC distance from N-Cadherin, a marker of localization of the adhesion complex. Yet, whether phosphorylation of RyR2 in PKP2cKO-RV myocytes is a determinant of RyR2 calcium release remains to be defined.

We observed that SERCA2a protein (but not transcript) levels were decreased, primarily in RV. The latter may play a role in the prolongation of the time constant of recovery in the Ca^{2+} transients. Moreover, we saw no difference in NCX function at fixed $[Ca^{2+}]$, though dynamic changes may occur. It is known that Cx43 hemichannels allow for entry not only of Ca^{2+} but also Na^{+}. Increased $[Na^{+}]_i$ would retard the forward mode activity of the Na^{+}-Ca^{2+} exchanger, further favoring Ca^{2+} accumulation in the intracellular space. Overall, the activity of NCX to extrude Ca^{2+} would be outmatched by persistent intake of external Ca^{2+} (and perhaps, Na^{+}) through Cx43 hemichannels, reaching a steady-state at higher levels of $[Ca^{2+}]_i$; this imbalance (or new balance) would be corrected by inhibition or ablation of Cx43. In terms of the relation between RyR2 abundance and function, reduced RyR2 levels may be compensated by the organization of RyR2 units into super-clusters that facilitate calcium release[11–13]. The latter change was not asymmetric, indicating that it may be a substrate that facilitates but is not sufficient to alter Ca^{2+} release.

Previous echocardiographic analysis at 14 days post-TAM showed increased RV area in PKP2cKO hearts, an early sign of changes in RV contractility[3]. Partial ablation of Cx43 mitigated this event, likely through normalization of $[Ca^{2+}]_i$; whether contractile dysfunction is consequent to Ca^{2+} dysregulation remains to be determined, though an association between Ca^{2+} homeostasis and contractility is well documented[43]. Alternatively, we speculate that the increased RV area is an early manifestation of impaired mechanical forces at the cellular level, combined with the differences in force distribution in various areas of the heart. At the cell level, Broussard et al have shown that impairing the association of desmosomes with intermediate filaments leads to decreased cell tension and stiffness[44]. One can surmise that at the tissue level, these changes would reflect on a weakened ventricular wall, leading to dilation. While the change in cell stiffness may (or may not) be generalized,

the forces impacting the ventricular wall are not evenly distributed throughout the heart; recent studies show, for example, that the thin-walled RV (and in particular the RVOT) is exposed to a particularly high wall shear stress[45]. Along these lines, echocardiographic analysis has documented impaired contractility and stiffness of the RV myocardium prior to LV dysfunction in subclinical ARVC patients that present with no evidence of fibrosis by late enhancement MRI.[46] The latter observation, all major differences notwithstanding, is consistent with the increased RV area in the 14 day post-TAM mice, which precedes overt fibrosis. At the cellular level, these uneven physical forces may cause the RV cells to be first to separate from each other, allowing increased entry of Ca^{2+} that in turn, may further impair the contractile function of the cells. Yet, it is important to recognize the role of Wnt-signalling-dependent embryonic programming as potential substrate for asymmetric differences, particularly in case of desmosomal deficiency [47].

Altogether, we propose that loss of PKP2 expression occurs in both ventricles but first affects RV desmosomal integrity. Loss of desmosomal integrity triggers two relatively unrelated events: a) Loss of stability of neighboring gap junctions, with consequent increase in orphan Cx43 hemichannels at the perinexus, and b) dislodgement of a kinase (likely PKC) from the intercalated disc, which translocates to phosphorylate an off-target substrate (RyR2-T2809), changing RyR2 gating properties. These two arms converge to a) facilitate development of potentially lethal arrhythmias and b) as time progresses, alter the transcriptional program of the cells and myocyte integrity, leading to arrhythmogenic cardiomyopathy.

Of note, we acknowledge that the mechanisms of arrhythmias may include additional events not yet detected by our experiments. Though we see cellular events that can be arrhythmogenic, and we do see arrhythmias, we do not argue that the arrhythmias are only and exclusively resulting from Ca^{2+} alterations.

We focused on PKP2 because of its importance in cardiac biology. Mutations in PKP2 associate with a pleiotropic disease (ARVC) that presents an electrical phenotype sometimes preceding and sometimes concurrent with a cardiomyopathy. It is worth noting that sudden death is the first disease manifestation in 11% of ARVC probands[5], and that a number of ARVC cases present mostly an electrical phenotype while the structural disease is concealed[5–7] or not present[48]. This coincides with the observation in our mice, indicating alterations in Ca^{2+} homeostasis well-known as potentially arrhythmogenic[3] as first detectable manifestation, prior to collagen accumulation. It is tempting to speculate that elevation of $[Ca^{2+}]_i$ can be a trigger for subsequent structural disease and the modified transcriptional program of the heart. Under that scenario, the elevated $[Ca^{2+}]_i$ would exert first an arrhythmogenic effect, followed by changes that take more time to manifest, namely, the transcriptional and structural events. Interestingly, despite the elevated $[Ca^{2+}]_i$ we did not detect signs of hypertrophy. This and other observations have led us to postulate the hypothesis (yet to be tested) that loss of PKP2 blunts activation of the transcriptional program necessary for compensatory hypertrophy.

We recognize that weaknesses remain regarding the mechanisms proposed. We have not studied quantitatively the relation between the Cx43-dependent permeability observed in our

tissue preparations (demonstrated by the passage of LY) and the $[Ca^{2+}]_i$ as it is measured in the single cells. It is important to note though that experimental conditions differ; in particular, the LY experiment is carried out in the absence of external Ca^{2+} added. This manipulation allows us to see the increased Cx43-dependent membrane permeability within the time frame of our recordings. But the natural time course of the increased $[Ca^{2+}]_i$ as it wold occur in the heart, remains to be determined. Also, related to the point above, we lack a quantitative description of the magnitude of the Ca^{2+} influx taking into account the limited permeability and the presumably low number of C43 hemichannels. In this regard, it is worth noting the study of John et al[49]. These authors calculated that in a cardiomyocyte, 10 open Cx43 hemichannels producing a 100 pA current at −80 mV would increase Na^+ influx by 75%. This would still represent a small fraction of a total of 2.6×10^6 junctional connexins estimated to be present in the myocyte and yet, the increase in intracellular Na^+ may favor an increase in $[Ca^{2+}]_i$. The amount of open hemichannels at one particular snapshot in time would be minimal, not causing a major impact to the cardiomyocyte membrane potential. Yet, the long-term effect of this Cx43 flickering would be the accumulation of Ca^{2+} in the intracellular space. Overall, our data strongly support the notion that a Cx43-dependent membrane conduit is necessary for the increased $[Ca^{2+}]_i$ reported; yet, how the various Ca^{2+} and Na^+ fluxes, through the various membrane compartments, balance to yield high $[Ca^{2+}]_i$ levels, remains to be determined.

While our observations are consistent with those in humans with ARVC, any extrapolation needs to be taken with caution, as it is clear that animal models do not reproduce the conditions of a patient with the disease. This is in fact true for all animal or cellular models of ARVC that have been published, and an obvious consequence of the limitations inherent to the study of a human disease. The significance of our studies is not in having reproduced conditions that lead to human ARVC, but in having studied a molecule that, when mutated, causes the disease. Whether the molecular steps described here occur in human hearts with PKP2 mutations remains undefined. Yet, it is worth mentioning that agents that block release of Ca^{2+} through RyR2 channels, such as flecainide, may be a possible combination therapy for ARVC patients[50], and that recent reports indicate that patients with first diagnosis of CPVT have been later identified as carriers of PKP2 mutations[48]. The relation between ARVC and Ca^{2+} mishandling is emphasized by the fact that mutations in phospholamban, a known contributor to Ca^{2+} homeostasis, can cause ARVC[5, 7]. We show a functional intersection of PKP2 and Ca^{2+} homeostasis and propose a model as to the steps by which one event (loss of intercellular adhesion at the intercalated disc) affects another (Ca^{2+} release) even though they are functions structurally separate in the myocyte space.

Supplementary Material

Refer to Web version on PubMed Central for supplementary material.

ACKNOWLEDGMENTS

The authors acknowledge the excellent support of Joseph Sall and Chris Petzold for EM sample preparation and image acquisition.

FUNDING SOURCES

This work was supported by grants RO1 HL134328, RO1 HL136179, RO1 HL145911 and a Fondation Leducq Transatlantic Network (MD), grant 18TPA34230006 (MC), 19CDA34660208 (FJA) from the American Heart Association, grant 2017R1E1A1A01074504 from the National Research Foundation of Korea (JCK), grants NIH RO1-HL055438 and RO1-HL134344 (HHV), grant NIH S10 ODO019974 (F-XL), grants DFF-6110-00166 and DFF-4092-00045 from The Danish Council for independent Research and NNF18OC0052844 from The Novo Nordisk Foundation (AL) and an Excellence Scholarship from the Rafael del Pino Foundation (MP-H). The NYU Microscopy shared resource is supported by Cancer Center Grant P30CA016087.

REFERENCES

1. Chen SN, Gurha P, Lombardi R, Ruggiero A, Willerson JT and Marian AJ. The hippo pathway is activated and is a causal mechanism for adipogenesis in arrhythmogenic cardiomyopathy. Circ Res. 2014;114:454–468. [PubMed: 24276085]
2. Bass-Zubek AE, Hobbs RP, Amargo EV, Garcia NJ, Hsieh SN, Chen X, Wahl JK 3rd, Denning MF and Green KJ. Plakophilin 2: a critical scaffold for PKC alpha that regulates intercellular junction assembly. J Cell Biol. 2008;181:605–613. [PubMed: 18474624]
3. Cerrone M, Montnach J, Lin X, Zhao YT, Zhang M, Agullo-Pascual E, Leo-Macias A, Alvarado FJ, Dolgalev I, Karathanos TV, Malkani K, Van Opbergen CJM, van Bavel JJA, Yang HQ, Vasquez C, Tester D, Fowler S, Liang F, Rothenberg E, Heguy A, Morley GE, Coetzee WA, Trayanova NA, Ackerman MJ, van Veen TAB, Valdivia HH and Delmar M. Plakophilin-2 is required for transcription of genes that control calcium cycling and cardiac rhythm. Nature communications. 2017;8:106.
4. Dubash AD, Kam CY, Aguado BA, Patel DM, Delmar M, Shea LD and Green KJ. Plakophilin-2 loss promotes TGF-beta1/p38 MAPK-dependent fibrotic gene expression in cardiomyocytes. J Cell Biol. 2016;212:425–438. [PubMed: 26858265]
5. Groeneweg JA, Bhonsale A, James CA, te Riele AS, Dooijes D, Tichnell C, Murray B, Wiesfeld AC, Sawant AC, Kassamali B, Atsma DE, Volders PG, de Groot NM, de Boer K, Zimmerman SL, Kamel IR, van der Heijden JF, Russell SD, Jan Cramer M, Tedford RJ, Doevendans PA, van Veen TA, Tandri H, Wilde AA, Judge DP, van Tintelen JP, Hauer RN and Calkins H. Clinical Presentation, Long-Term Follow-Up, and Outcomes of 1001 Arrhythmogenic Right Ventricular Dysplasia/Cardiomyopathy Patients and Family Members. Circulation Cardiovascular genetics. 2015;8:437–446. [PubMed: 25820315]
6. Delmar M and McKenna WJ. The cardiac desmosome and arrhythmogenic cardiomyopathies: from gene to disease. Circ Res. 2010;107:700–714. [PubMed: 20847325]
7. Corrado D, Link MS and Calkins H. Arrhythmogenic Right Ventricular Cardiomyopathy. N Engl J Med. 2017;376:61–72. [PubMed: 28052233]
8. Liao Y, Day KH, Damon DN and Duling BR. Endothelial cell-specific knockout of connexin 43 causes hypotension and bradycardia in mice. Proc Natl Acad Sci U S A. 2001;98:9989–9994. [PubMed: 11481448]
9. Hulsmans M, Clauss S, Xiao L, Aguirre AD, King KR, Hanley A, Hucker WJ, Wulfers EM, Seemann G, Courties G, Iwamoto Y, Sun Y, Savol AJ, Sager HB, Lavine KJ, Fishbein GA, Capen DE, Da Silva N, Miquerol L, Wakimoto H, Seidman CE, Seidman JG, Sadreyev RI, Naxerova K, Mitchell RN, Brown D, Libby P, Weissleder R, Swirski FK, Kohl P, Vinegoni C, Milan DJ, Ellinor PT and Nahrendorf M. Macrophages Facilitate Electrical Conduction in the Heart. Cell. 2017;169:510–522 e20. [PubMed: 28431249]
10. Takefuji M, Wirth A, Lukasova M, Takefuji S, Boettger T, Braun T, Althoff T, Offermanns S and Wettschureck N. G(13)-mediated signaling pathway is required for pressure overload-induced cardiac remodeling and heart failure. Circulation. 2012;126:1972–1982. [PubMed: 22972902]
11. Macquaide N, Tuan HT, Hotta J, Sempels W, Lenaerts I, Holemans P, Hofkens J, Jafri MS, Willems R and Sipido KR. Ryanodine receptor cluster fragmentation and redistribution in persistent atrial fibrillation enhance calcium release. Cardiovasc Res. 2015;108:387–398. [PubMed: 26490742]
12. Galice S, Xie Y, Yang Y, Sato D and Bers DM. Size Matters: Ryanodine Receptor Cluster Size Affects Arrhythmogenic Sarcoplasmic Reticulum Calcium Release. J Am Heart Assoc. 2018;7:e008724. [PubMed: 29929992]

13. Kolstad TR, van den Brink J, MacQuaide N, Lunde PK, Frisk M, Aronsen JM, Norden ES, Cataliotti A, Sjaastad I, Sejersted OM, Edwards AG, Lines GT and Louch WE. Ryanodine receptor dispersion disrupts Ca(2+) release in failing cardiac myocytes. Elife. 2018;7:e39427. [PubMed: 30375974]
14. Xie Y, Yang Y, Galice S, Bers DM and Sato D. Size Matters: Ryanodine Receptor Cluster Size Heterogeneity Potentiates Calcium Waves. Biophys J. 2019;116:530–539. [PubMed: 30686487]
15. Agullo-Pascual E, Lin X, Leo-Macias A, Zhang M, Liang FX, Li Z, Pfenniger A, Lubkemeier I, Keegan S, Fenyo D, Willecke K, Rothenberg E and Delmar M. Super-resolution imaging reveals that loss of the C-terminus of connexin43 limits microtubule plus-end capture and NaV1.5 localization at the intercalated disc. Cardiovasc Res. 2014;104:371–381. [PubMed: 25139742]
16. Ullrich ND, Valdivia HH and Niggli E. PKA phosphorylation of cardiac ryanodine receptor modulates SR luminal Ca2+ sensitivity. J Mol Cell Cardiol. 2012;53:33–42. [PubMed: 22487381]
17. Liu B, Ho HT, Velez-Cortes F, Lou Q, Valdivia CR, Knollmann BC, Valdivia HH and Gyorke S. Genetic ablation of ryanodine receptor 2 phosphorylation at Ser-2808 aggravates Ca(2+)-dependent cardiomyopathy by exacerbating diastolic Ca2+ release. J Physiol. 2014;592:1957–1973. [PubMed: 24445321]
18. Camors E and Valdivia HH. CaMKII regulation of cardiac ryanodine receptors and inositol triphosphate receptors. Front Pharmacol. 2014;5:101. [PubMed: 24847270]
19. Lundby A, Rossin EJ, Steffensen AB, Acha MR, Newton-Cheh C, Pfeufer A, Lynch SN, Consortium QTIIG, Olesen SP, Brunak S, Ellinor PT, Jukema JW, Trompet S, Ford I, Macfarlane PW, Krijthe BP, Hofman A, Uitterlinden AG, Stricker BH, Nathoe HM, Spiering W, Daly MJ, Asselbergs FW, van der Harst P, Milan DJ, de Bakker PI, Lage K and Olsen JV. Annotation of loci from genome-wide association studies using tissue-specific quantitative interaction proteomics. Nat Methods. 2014;11:868–874. [PubMed: 24952909]
20. Yuchi Z, Lau K and Van Petegem F. Disease mutations in the ryanodine receptor central region: crystal structures of a phosphorylation hot spot domain. Structure. 2012;20:1201–1211. [PubMed: 22705209]
21. Rust HL and Thompson PR. Kinase consensus sequences: a breeding ground for crosstalk. ACS Chem Biol. 2011;6:881–892. [PubMed: 21721511]
22. Peng W, Shen H, Wu J, Guo W, Pan X, Wang R, Chen SR and Yan N. Structural basis for the gating mechanism of the type 2 ryanodine receptor RyR2. Science. 2016;354:301.
23. Lipp P, Huser J, Pott L and Niggli E. Subcellular properties of triggered Ca2+ waves in isolated citrate-loaded guinea-pig atrial myocytes characterized by ratiometric confocal microscopy. J Physiol. 1996;497:599–610. [PubMed: 9003547]
24. Nilbratt M, Porras O, Marutle A, Hovatta O and Nordberg A. Neurotrophic factors promote cholinergic differentiation in human embryonic stem cell-derived neurons. J Cell Mol Med. 2010;14:1476–1484. [PubMed: 19799651]
25. Trollinger DR, Cascio WE and Lemasters JJ. Selective loading of Rhod 2 into mitochondria shows mitochondrial Ca2+ transients during the contractile cycle in adult rabbit cardiac myocytes. Biochem biophys res commun. 1997;236:738–742. [PubMed: 9245725]
26. Kim JC, Wang J, Son MJ, Cuong NM and Woo SH. Sensitization of cardiac Ca(2+) release sites by protein kinase C signaling: evidence from action of murrayafoline A. Pflugers Arch. 2015;467:1607–1621. [PubMed: 25095987]
27. Kostin S, Hein S, Bauer EP and Schaper J. Spatiotemporal development and distribution of intercellular junctions in adult rat cardiomyocytes in culture. Circ Res. 1999;85:154–167. [PubMed: 10417397]
28. Danik SB, Liu F, Zhang J, Suk HJ, Morley GE, Fishman GI and Gutstein DE. Modulation of cardiac gap junction expression and arrhythmic susceptibility. Circ Res. 2004;95:1035–1041. [PubMed: 15499029]
29. Gutstein DE, Morley GE, Tamaddon H, Vaidya D, Schneider MD, Chen J, Chien KR, Stuhlmann H and Fishman GI. Conduction slowing and sudden arrhythmic death in mice with cardiac-restricted inactivation of connexin43. Circ Res. 2001;88:333–339. [PubMed: 11179202]

30. Eckardt D, Theis M, Degen J, Ott T, van Rijen HV, Kirchhoff S, Kim JS, de Bakker JM and Willecke K. Functional role of connexin43 gap junction channels in adult mouse heart assessed by inducible gene deletion. J Mol Cell Cardiol. 2004;36:101–110. [PubMed: 14734052]
31. Wang N, De Vuyst E, Ponsaerts R, Boengler K, Palacios-Prado N, Wauman J, Lai CP, De Bock M, Decrock E, Bol M, Vinken M, Rogiers V, Tavernier J, Evans WH, Naus CC, Bukauskas FF, Sipido KR, Heusch G, Schulz R, Bultynck G and Leybaert L. Selective inhibition of Cx43 hemichannels by Gap19 and its impact on myocardial ischemia/reperfusion injury. Basic Res Cardiol. 2013;108:309. [PubMed: 23184389]
32. Gadicherla AK, Wang N, Bulic M, Agullo-Pascual E, Lissoni A, De Smet M, Delmar M, Bultynck G, Krysko DV, Camara A, Schluter KD, Schulz R, Kwok WM and Leybaert L. Mitochondrial Cx43 hemichannels contribute to mitochondrial calcium entry and cell death in the heart. Basic Res Cardiol. 2017;112:127.
33. Cerrone M, Lin X, Zhang M, Agullo-Pascual E, Pfenniger A, Chkourko Gusky H, Novelli V, Kim C, Tirasawadichai T, Judge DP, Rothenberg E, Chen HS, Napolitano C, Priori SG and Delmar M. Missense mutations in plakophilin-2 cause sodium current deficit and associate with a brugada syndrome phenotype. Circulation. 2014;129:1092–1103. [PubMed: 24352520]
34. van Berlo JH, Maillet M and Molkentin JD. Signaling effectors underlying pathologic growth and remodeling of the heart. J Clin Invest. 2013;123:37–45. [PubMed: 23281408]
35. Gomez AM, Ruiz-Hurtado G, Benitah JP and Dominguez-Rodriguez A. Ca(2+) fluxes involvement in gene expression during cardiac hypertrophy. Curr Vasc Pharmacol. 2013;11:497–506. [PubMed: 23905644]
36. Rhett JM, Jourdan J and Gourdie RG. Connexin 43 connexon to gap junction transition is regulated by zonula occludens-1. Mol Biol Cell. 2011;22:1516–1528. [PubMed: 21411628]
37. Verma V, Hallett MB, Leybaert L, Martin PE and Evans WH. Perturbing plasma membrane hemichannels attenuates calcium signalling in cardiac cells and HeLa cells expressing connexins. Eur J Cell Biol. 2009;88:79–90. [PubMed: 18951659]
38. Contreras JE, Saez JC, Bukauskas FF and Bennett MV. Gating and regulation of connexin 43 (Cx43) hemichannels. Proc Natl Acad Sci U S A. 2003;100:11388–11393. [PubMed: 13130072]
39. Cerrone M, van Opbergen CJM, Malkani K, Irrera N, Zhang M, Van Veen TAB, Cronstein B and Delmar M. Blockade of the Adenosine 2A Receptor Mitigates the Cardiomyopathy Induced by Loss of Plakophilin-2 Expression. Front Physiol. 2018;9:1750. [PubMed: 30568602]
40. Saffitz JE. Arrhythmogenic cardiomyopathy and abnormalities of cell-to-cell coupling. Heart Rhythm. 2009;6:S62–S65.
41. Asimaki A and Saffitz JE. Remodeling of cell-cell junctions in arrhythmogenic cardiomyopathy. Cell Commun Adhes. 2014;21:13–23. [PubMed: 24460198]
42. Oxford EM, Musa H, Maass K, Coombs W, Taffet SM and Delmar M. Connexin43 remodeling caused by inhibition of plakophilin-2 expression in cardiac cells. Circ Res. 2007;101:703–711. [PubMed: 17673670]
43. Eisner DA, Caldwell JL, Kistamas K and Trafford AW. Calcium and Excitation-Contraction Coupling in the Heart. Circ Res. 2017;121:181–195. [PubMed: 28684623]
44. Broussard JA, Yang R, Huang C, Nathamgari SSP, Beese AM, Godsel LM, Hegazy MH, Lee S, Zhou F, Sniadecki NJ, Green KJ and Espinosa HD. The desmoplakin-intermediate filament linkage regulates cell mechanics. Mol Biol Cell. 2017;28:3156–3164. [PubMed: 28495795]
45. Gulan U, Saguner AM, Akdis D, Gotschy A, Tanner FC, Kozerke S, Manka R, Brunckhorst C, Holzner M and Duru F. Hemodynamic Changes in the Right Ventricle Induced by Variations of Cardiac Output: A Possible Mechanism for Arrhythmia Occurrence in the Outflow Tract. Scientific reports. 2019;9:100. [PubMed: 30643204]
46. Mast TP, Teske AJ, Walmsley J, van der Heijden JF, van Es R, Prinzen FW, Delhaas T, van Veen TA, Loh P, Doevendans PA, Cramer MJ and Lumens J. Right Ventricular Imaging and Computer Simulation for Electromechanical Substrate Characterization in Arrhythmogenic Right Ventricular Cardiomyopathy. J Am Coll Cardiol. 2016;68:2185–2197. [PubMed: 27855808]
47. Li G, Khandekar A, Yin T, Hicks SC, Guo Q, Takahashi K, Lipovsky CE, Brumback BD, Rao PK, Weinheimer CJ and Rentschler SL. Differential Wnt-mediated programming and arrhythmogenesis in right versus left ventricles. J Mol Cell Cardiol. 2018;123:92–107. [PubMed: 30193957]

48. Tester DJ, Ackerman JP, Giudicessi JR, Ackerman NC, Cerrone M, Delmar M and Ackerman MJ. Plakophilin-2 Truncation Variants in Patients Clinically Diagnosed With Catecholaminergic Polymorphic Ventricular Tachycardia and Decedents With Exercise-Associated Autopsy Negative Sudden Unexplained Death in the Young. JACC Clin Electrophysiol. 2019;5:120–127. [PubMed: 30678776]

49. John SA, Kondo R, Wang SY, Goldhaber JI and Weiss JN. Connexin-43 hemichannels opened by metabolic inhibition. J Biol Chem. 1999;274:236–240. [PubMed: 9867835]

50. Ermakov S, Gerstenfeld EP, Svetlichnaya Y and Scheinman MM. Use of flecainide in combination antiarrhythmic therapy in patients with arrhythmogenic right ventricular cardiomyopathy. Heart Rhythm. 2017;14:564–569. [PubMed: 27939893]

CLINICAL PERSPECTIVE

What is new?

- This is the first demonstration that loss of Plakophilin-2 expression causes, as an early event and predominantly in the right ventricle (RV), a non-transcriptional, likely arrhythmogenic, Connexin43-dependent disruption of Ca^{2+}_i homeostasis.
- The phenotype includes accumulation of Ca^{2+} in three intracellular compartments: the junctional sarcoplasmic reticulum (SR), the cytoplasm, and the mitochondria; RV myocytes also show increased eagerness of RyR2 channels to release Ca^{2+} from the SR.
- Intrinsic RyR2 properties are also modified; specifically, RV RyR2 channels have enhanced sensitivity to Ca^{2+} and are selectively phosphorylated (likely by PKC) at residue T2809, further contributing to the pro-arrhythmogenic state.

What are the clinical implications?

- Mutations in plakophilin-2 are the most common cause of gene-positive familial arrhythmogenic right ventricular cardiomyopathy (ARVC).
- We postulate that disruption of Ca^{2+}_i homeostasis in the RV is a major arrhythmia trigger in patients with ARVC.
- Our data identifies both the RyR2 channel and the Cx43 hemichannel as targets for antiarrhythmic therapy in the afflicted population.

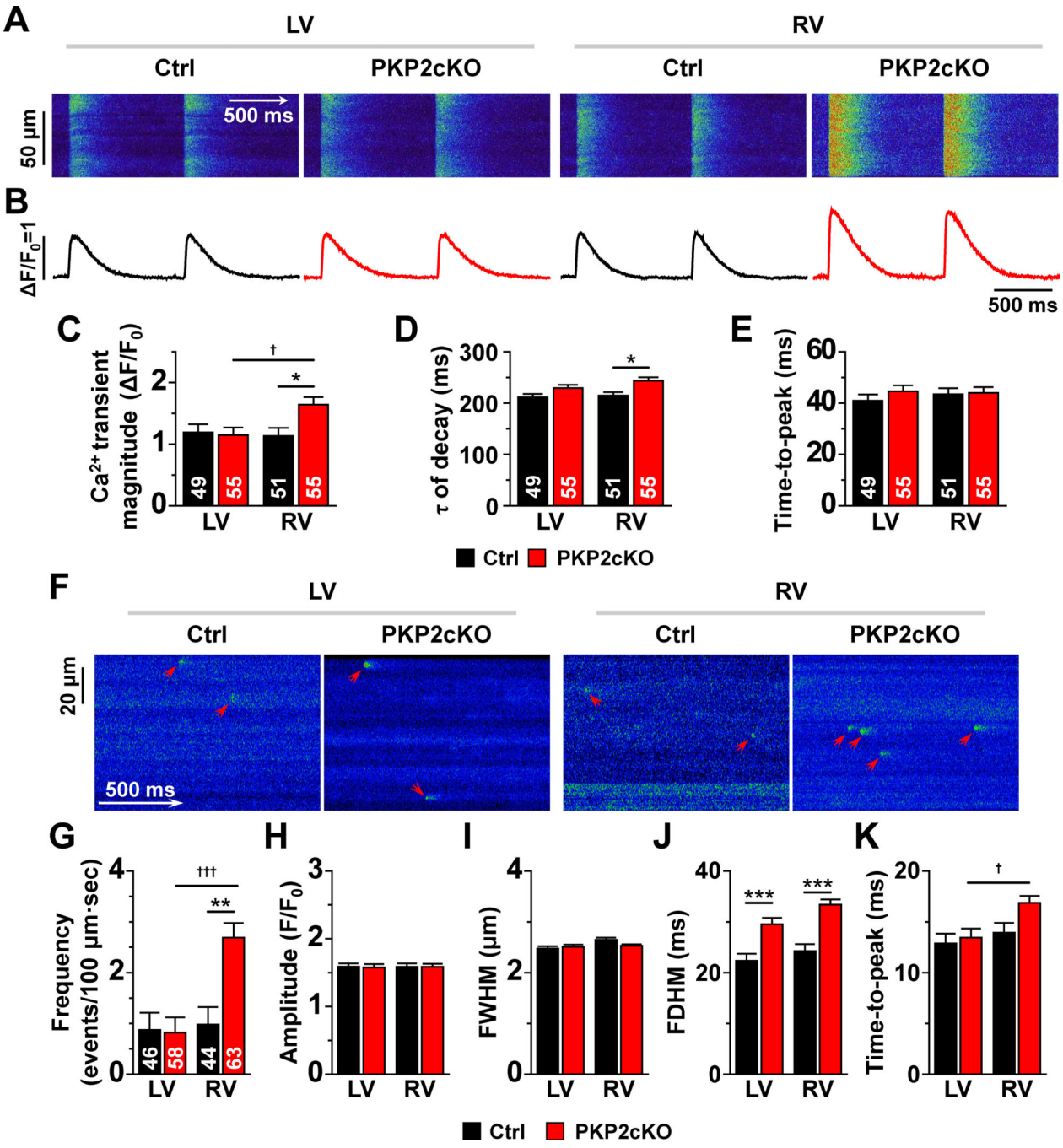

Figure 1. Ca^{2+} transients and Ca^{2+} sparks in RV and LV myocytes from control and PKP2cKO hearts.

Time-space plots (**A**) and time course of Ca^{2+} transients (**B**) obtained by line-scans (1.43 ms/line) during field stimulation (1 Hz) of myocytes isolated from the left ventricle (LV) and right ventricle (RV) of control (Ctrl) and plakophilin-2 conditional knockout (PKP2cKO) mice. Panels C-E show compiled data for mean Ca^{2+} transient magnitude (relative amplitude; $\Delta F/F_0$; **C**), time constant of Ca^{2+} transient decay (ms; **D**) and time-to-peak (ms; **E**). Black and red bars depict data from Ctrl and PKP2cKO myocytes, respectively. **Panel F**:

confocal line-scan images of Ca^{2+} sparks (green; emphasized by red arrowheads) recorded from control (Ctrl) and PKP2cKO myocytes isolated from either LV or RV. Cumulative data are shown in panels G-K. Black and red bars represent data obtained from control and PKP2cKO mice, respectively. **G:** Mean frequency of Ca^{2+} sparks, reported as average number of events per second in a 100 μm line. **H**: Average peak amplitude (F/F_0). **I**: full-width at half maximum (FWHM; μm). **J**: full duration at half maximum (FDHM; ms). **K**: time-to-peak (ms). For all bar graphs: black, control; red, PKP2cKO. Number of cells studied are noted in the corresponding bars. For panels C-E: Statistical tests: Hierarchical test was first attempted. Output indicated whether to proceed via two-way repeated measures analysis of variance (ANOVA)-Bonferroni (details in “Methods”). Hierarchical test used for transient amplitude. Two-way repeated measures ANOVA-Bonferroni for tau and time to peak. Total mice: 9 controls and 11 PKP2cKO. *p<0.05 vs. control, $^{\dagger}p$<0.05 vs. LV. For panels G-K: Numbers of sparks/cells/mice in control dataset: 618 sparks from 46 LV cells; 594 sparks from 44 RV cells; 6 mice. Numbers of sparks/cells/mice in PKP2cKO dataset: 675 sparks from 58 LV cells; 1842 sparks from 63 RV cells; 7 mice. Statistical test: Hierarchical analysis. See “Methods” for details. **p<0.01 vs. control; ***p<0.001 vs. control; $^{\dagger}p$<0.05 vs. LV; $^{\dagger\dagger\dagger}p$<0.001 vs. LV.

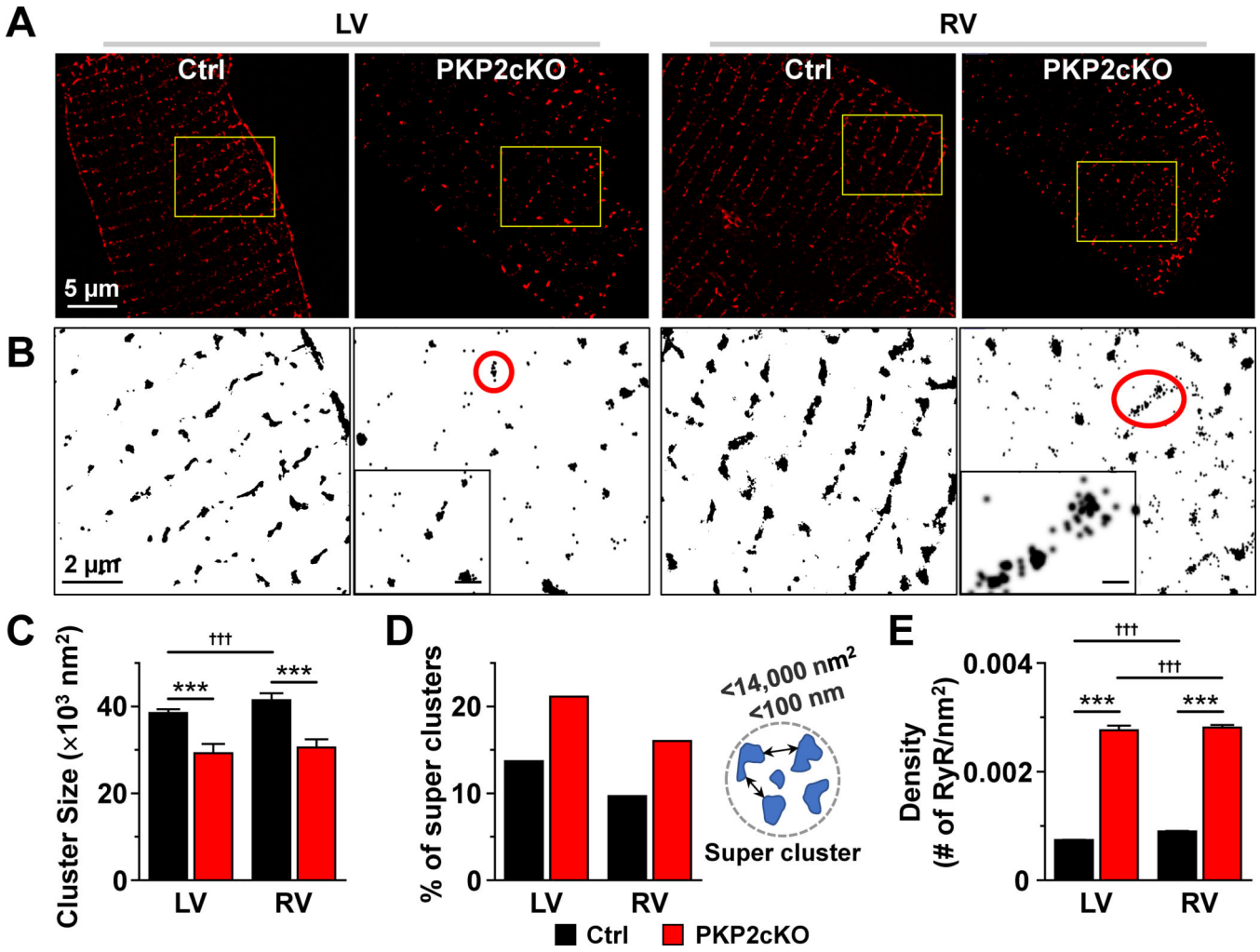

Figure 2. Analysis of RyR2 clustering using single molecule-localization microscopy (SMLM).

A: Stochastic optical reconstruction microscopy (STORM)-acquired images of ryanodine receptor 2 (RyR2) in single myocytes dissociated from left ventricle (LV) or right ventricle (RV) of control (Ctrl) or plakophilin-2 conditional knockout (PKP2cKO) mice 14 days post-TAM. **B**: Yellow-boxed areas in A are shown in black and white for better visualization. Clusters within red circles in PKP2cKO are shown at larger magnification in the inset to illustrate the organization of small clusters in close proximity (scale bar in insets, 200 nm). **C**: Average size of RyR2 clusters in control and PKP2cKO myocytes. Control: n=24158 clusters from 11 LV cells; 14906 clusters from 8 RV cells. PKP2cKO: n=27365 clusters from 19 LV cells; 31852 clusters from 18 RV cells. **D**: Bar graph shows the proportion of super-clusters in control or PKP2cKO myocytes. LV control: 3280 super-clusters/23946 total clusters; LV PKP2cKO: 1581 super-clusters/7481 total clusters; RV control: 1435 super-clusters/14815 total clusters; RV PKP2cKO: 1534 super-clusters/9586 total clusters. Criteria used for defining super-clusters is diagrammed at the right of the panel. **E**: RyR2 molecular density, estimated as the number of RyR2 molecules (calculated by Density-Based Spatial Clustering of Applications with Noise; DBSCAN) per unit of cluster area (see also Methods). Number of clusters analyzed (including clusters with at least 10 RyRs): 32738

LV and 16595 RV clusters from control; 1666 LV and 4396 RV clusters from PKP2cKO. Statistical significance by two-way repeated measures analysis of variance (ANOVA)-Bonferroni test, ***$p<0.001$ vs. control. $^{\dagger\dagger\dagger}p<0.001$ vs. LV.

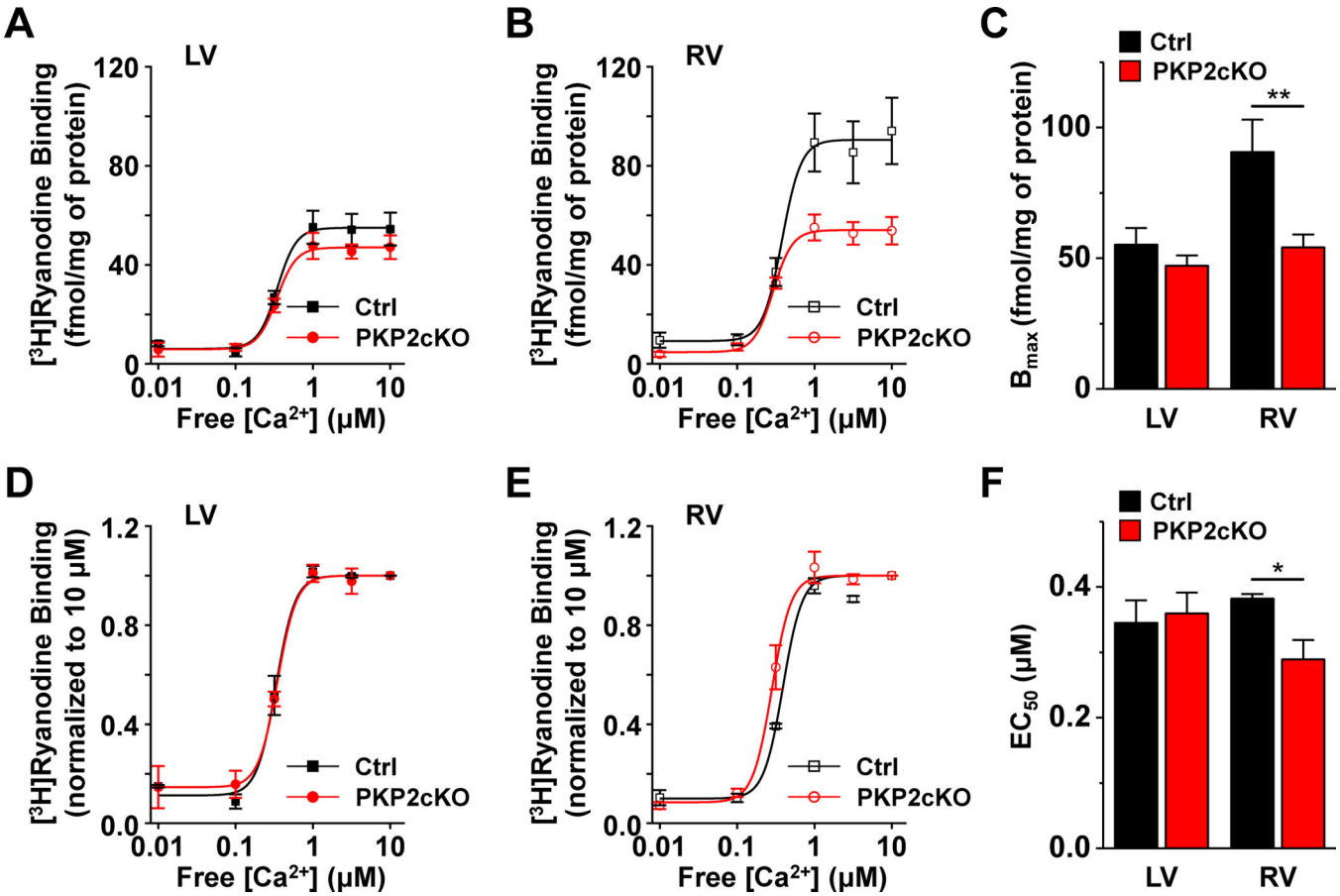

Figure 3. [^{3}H]Ryanodine binding in homogenates from control or PKP2cKO hearts.

A: [^{3}H]Ryanodine binding as a function of free [Ca^{2+}] in samples obtained from the left ventricle (LV) of either control (Ctrl) or plakophilin-2 conditional knockout (PKP2cKO) hearts 14 days post-TAM. **B**: Same as A but for samples obtained from the right ventricle (RV). Cumulative data for binding maximum (B_{max}) is shown in **C**. Data normalized for the binding observed at 10 μM free [Ca^{2+}] for LV and RV are shown in panels **D** and **E**, respectively. This correction allowed us to observe a shift in the concentration of free [Ca^{2+}] that produces 50% of maximal [^{3}H]Ryanodine binding (EC_{50}) in the RV tissue of PKP2cKO hearts (**F**). n=4 hearts for each group. *p<0.05 vs. control. **p<0.01 vs. control. Two-way repeated measures analysis of variance (ANOVA)–Bonferroni test.

A

Position	Phospho (STY) Probabilities
653	LVNHVS(1)S(1)MRPNIFLGVSEGSAQYK
654	LVNHVS(1)S(1)MRPNIFLGVSEGSAQYK
1399	TKPDYS(0.045)T(0.731)GHS(0.224)AR
1864	EAAVPEEEGGT(0.996)PEKEIS(0.004)IEDAK
1870	EIS(1)IEDAKLEGEEEAK
2367	IAEDPSRDGPSPT(0.002)S(0.04)GS(0.931)S(0.027)K
2693	QS(0.192)S(0.766)MDS(0.042)EGNFNPQPVDTSNITIPEK
2807	RIS(0.993)QT(0.007)SQVSIDAAHGYSPR
2809	IS(0.039)QT(0.944)S(0.017)QVSIDAAHGYSPR
2810	IS(0.063)QT(0.008)S(0.929)QVS(0.001)IDAAHGYSPR
2813	ISQTSQVS(1)IDAAHGYSPR

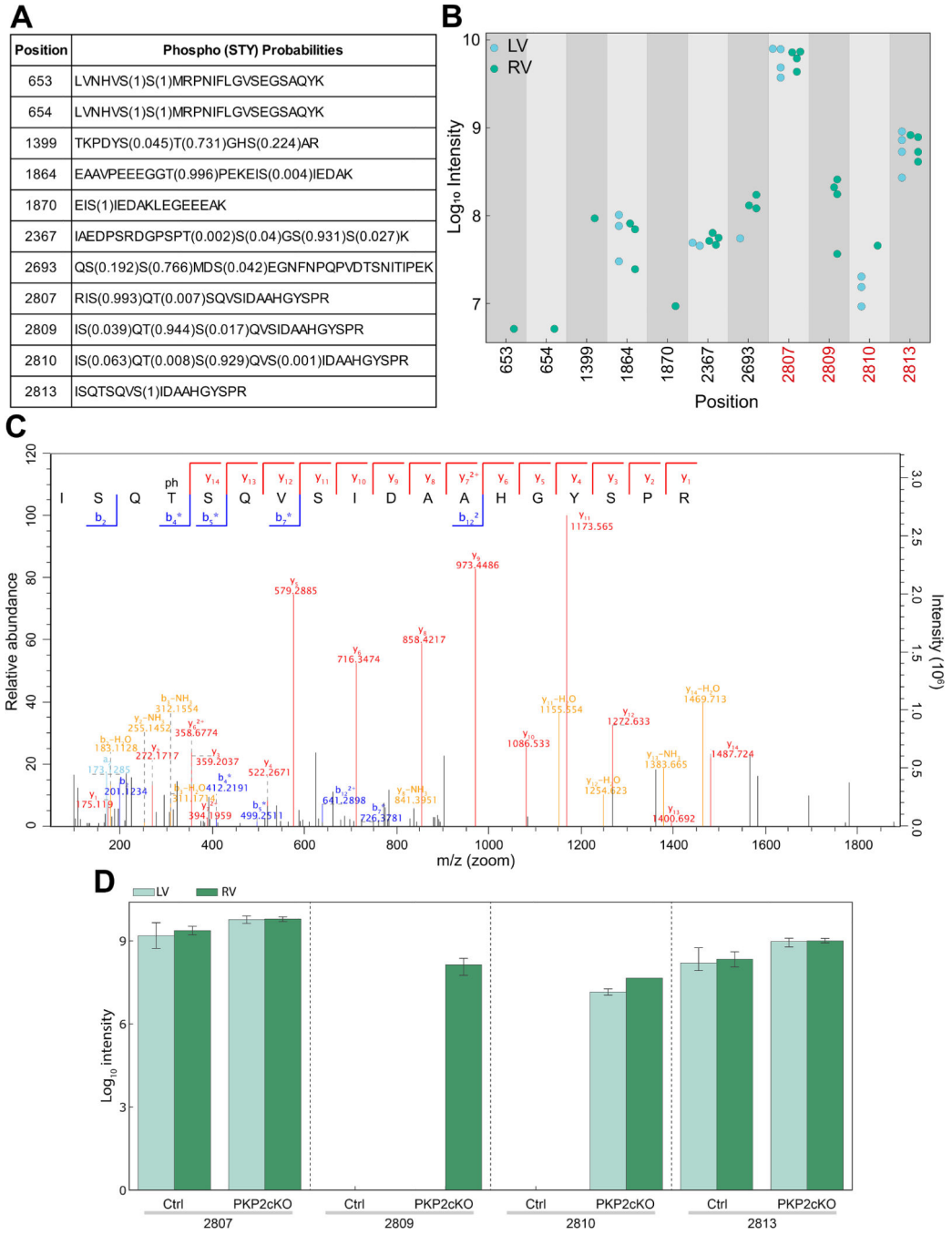

Figure 4. Mass spectrometry-based investigation of RyR2 phosphorylation state in LV versus RV of PKP2cKO hearts.

A: Summary of the eleven class-1 phosphopeptides identified. The first column indicates the position of the phosphorylated amino acid in the ryanodine receptor 2 (RyR2) sequence and the second column, the amino acid sequence of the peptide in which the phosphorylation site was measured. The numbers in brackets indicate the probability with which the localization of the phosphorylation site has been assigned to that particular residue (assignment of phosphorylation site localization depends on fragmentation pattern). **B**: Mass spectrometry-

based intensity measurements of phosphopeptides covering the eleven phosphorylation sites. Intensities of all measured phosphopeptides are displayed. Measurements from right ventricle (RV) samples are depicted in green and measurements from left ventricle (LV) samples, in blue. The phosphorylation 'hot spot' of RyR2 is highlighted in red. Phosphorylation of site 2809 was exclusively identified in RV samples. **C**: Measured peptide covering T2809 is shown along with the detected fragment ions indicated. The fragment ions are highlighted in the tandem mass spectrometry (MS/MS) spectrum. The peptide contained one phosphate group, and due to the fragmentation pattern the phosphorylation site could be localized to threonine 2809. **D**: Data summary. Mass-spectrometry based intensity measurements of phosphopeptides covering the four phosphorylation sites in the "hotspot" region of RyR2 from tissue samples control (Ctrl) and plakophilin-2 conditional knockout (PKP2cKO) mice. Measurements from LV and RV samples depicted in light and dark green, respectively. n=3 for control samples and 4 for PKP2cKO samples.

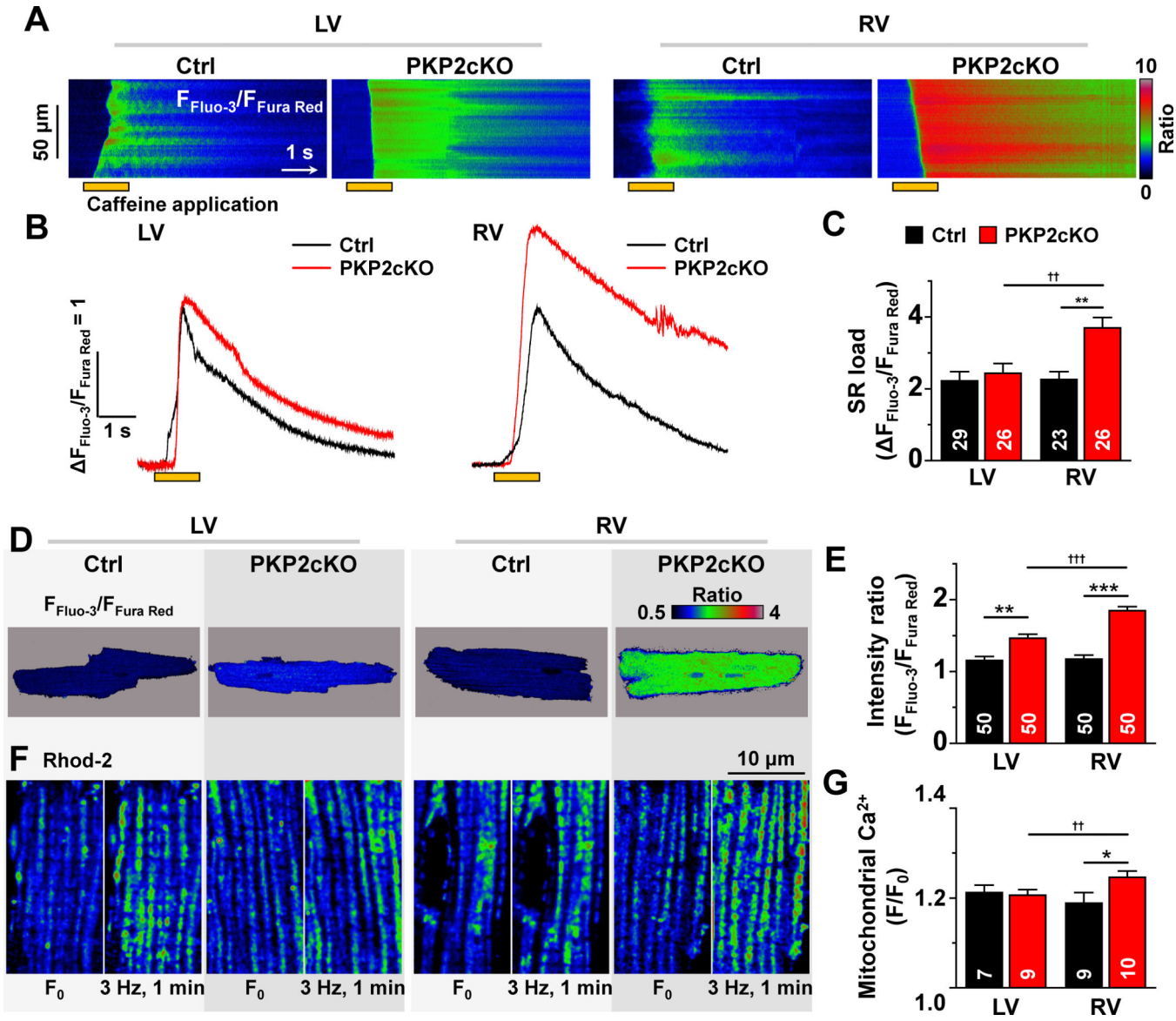

Figure 5. Ca^{2+} content in the intracellular compartments.

A: Confocal line-scan images (1.43 ms/line) recorded from non-permeabilized myocytes isolated from the free walls of the left ventricle (LV) or the right ventricle (RV) of either control (Ctrl) or plakophilin-2 conditional knockout (PKP2cKO) mice 14 days post-tamoxifen (post-TAM). In this and other panels, the pulse of caffeine (10 mM) is indicated by the orange bar at the bottom of the image. Intracellular calcium changes were detected by a ratiometric method ($F_{Fluo\text{-}3}/F_{Fura\ Red}$; see also "Methods"). **B:** Time course and amplitude of the change in fluorescence during and immediately following the caffeine pulse. Notice the larger amplitude of the transient recorded from PKP2cKO RV myocytes. Cumulative data are shown in **C**. Number of experiments noted in the bar graphs. Cells originated from 5 different mice in each group (Ctrl or PKP2cKO). Statistical test: Two-way repeated measures analysis of variance (ANOVA)-Bonferroni. Control: n=29 LV cells, 23 RV cells. PKP2cKO: n=26 LV cells, 26 RV cells. $^{**}p<0.01$ vs. control, $^{\dagger\dagger}p<0.01$ vs. LV. **D:** Pseudo-

colored confocal 2D images of the ratio of emission intensities ($F_{Fluo\text{-}3}/F_{Fura\ Red}$; see also "Methods"). The average of the calculated intensity ratios are shown in panel **E**. Statistical test: Hierarchical analysis. Control: n=50 LV cells, 50 RV cells from 5 mice. PKP2cKO n=50 LV cells, 50 RV cells from 5 mice. $^{**}p<0.01$ vs. control $^{***}p<0.001$ vs. control, $^{\dagger\dagger\dagger}p<0.001$ vs. LV. **F**: Confocal 2-D images of cardiomyocytes loaded with 2 μM Rhod 2-AM at low termperature (4°C) and then incubated at 37°C for 4 hours (see also "Methods"). For each group, two images from the same cell are shown: at rest (F_0; left), and after one minute stimulation at 3 Hz (right). Notice the increased number of fluorescence emission units (mitochondria) after stimulation, particularly in the cell from the PKP2cKO RV. **G:** Average of the ratio of Rhod-2 fluorescence intensities acquired before (F_0) and after (F) the period of pacing. Control (Ctrl): n=7 LV cells, 9 RV cells from 2 mice. PKP2cKO: n=9 LV cells, 10 RV cells from 2 mice. Statistical test: Two-way repeated measures ANOVA-Bonferroni. $^{*}p<0.05$ vs. control, $^{\dagger\dagger}p<0.01$ vs. LV.

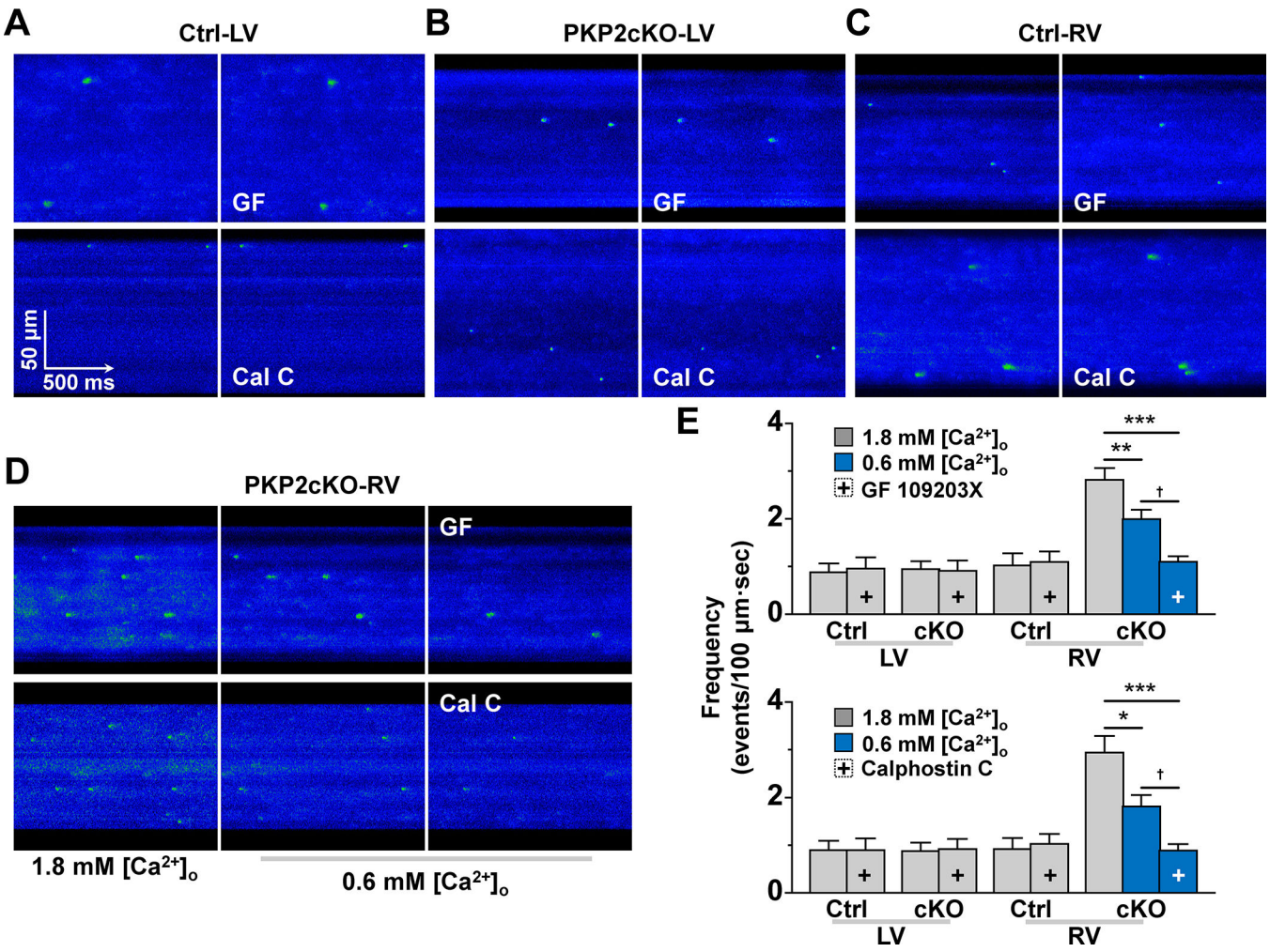

Figure 6. Spark frequency at equal sarcoplasmic reticulum (SR) load and effect of PKC inhibition.

A-D: confocal line-scan images of Ca^{2+} sparks (green) in Control (Ctrl; A and C) or plakophilin-2 conditional knockout (PKP2cKO) samples (B and D) obtained from the left ventricle (LV; A and B) or the right ventricle (RV; C and D). Panel D shows sparks obtained when cells were maintained in either 1.8 mM $[Ca^{2+}]_o$ (left) or in 0.6 mM $[Ca^{2+}]_o$ (middle and right panels). In panels A-D, right-most panel corresponds to data obtained in the presence of protein kinase C (PKC) inhibitors bisindolylmaleimide I (GF 109203X; labelled GF; top) or Calphostin C (labelled Cal C; bottom). **Panel E**: Spark (spontaneous calcium release or SCR) events measured under the various conditions. + indicates in the presence of the PKC inhibitor (GF 109203X in top panel; Calphostin C in bottom panel). Blue bars: data obtained at 0.6 mM $[Ca^{2+}]_o$. All experiments were carried out in sequence on the same cell: recordings at $[Ca^{2+}]_o$ 1.8 mM, then switched to 0.6 mM $[Ca^{2+}]_o$ (for PKP2cKO RV) and then addition of PKC inhibitor. Each group was treated separately and only one variable (SCR frequency) was measured. cKO means plakophilin-2 conditional knockout. Paired sample *t*-test for Control LV, Ctrl RV, PKP2cKO–LV (same cell compared before and after treatment). One-way repeated measures analysis of variance (ANOVA)-Bonferroni for PKP2cKO-RV (same cell compared at $[Ca^{2+}]_o$ 1.8 mM, then at 0.6 mM $[Ca^{2+}]_o$ and then

treatment). For experiments with GF 109203X: Control n=8 LV cells, 9 RV cells from 3 mice. PKP2cKO n=6 LV cells, 15 RV cells from 3 mice. **p<0.01. ***p<0.001 vs. 1.8 mM $[Ca^{2+}]_o$, $^{\dagger}p$<0.05 vs. 0.6 mM $[Ca^{2+}]_o$ For experiments with Calphostin C: Control n=9 LV cells, 7 RV cells from 3 mice. PKP2cKO n=11 LV cells, 13 RV cells from 3 mice. *p<0.05, ***p<0.001 vs. 1.8 mM $[Ca^{2+}]_o$, $^{\dagger}p$<0.05 vs. 0.6 mM $[Ca^{2+}]_o$.

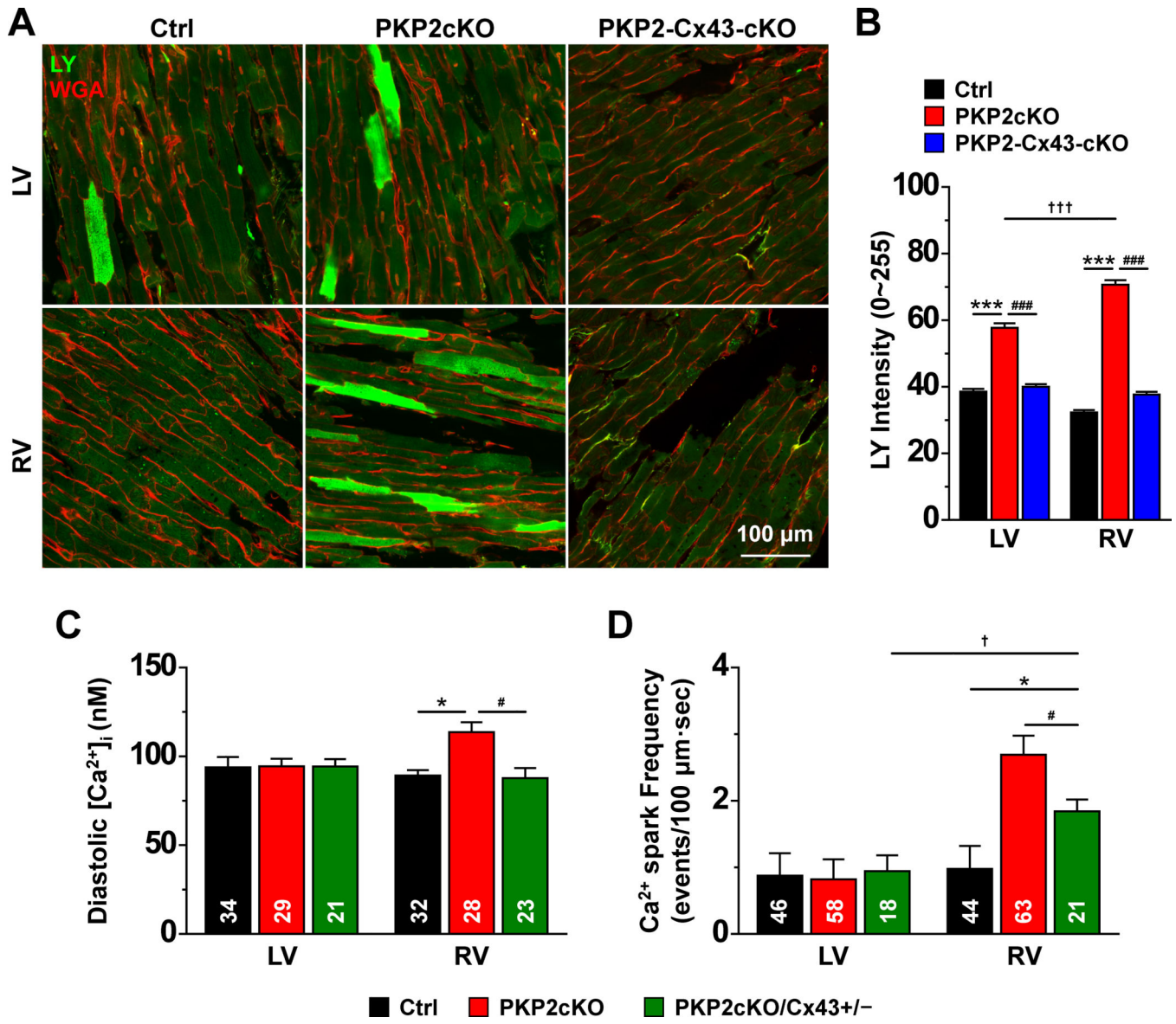

Figure 7. Membrane permeability to Lucifer Yellow and Cx43 expression.

A: Confocal images collected from the epicardial phase of either the free walls of the left ventricle (LV) or the right ventricle (RV) of hearts harvested from control (Ctrl), plakophilin-2 conditional knockout (PKP2cKO) mice 14 days post-tamoxifen (post-TAM) or a double knockout of PKP2 and Cx43, also at 14 days post-TAM (PKP2-Cx43-cKO). Images were obtained after a 30-min perfusion with 1 mg/mL Lucifer Yellow (LY; molecular weight 457; green), 1 mg/mL Rhodamine Dextran (molecular weight ~10,000) and 0.04 mg/mL Wheat Germ Agglutinin (WGA; red) in 10 nM free [Ca^{2+}] solution (see "Methods" for further details). Image fields were chosen at random and the intensity of the LY fluorescence (in a scale 0–225) was measured within regions of interest (ROIs) that excluded areas void of cells. **B**: Average LY intensity measured from cells in the following groups: Control (Ctrl; black bars; n=512 LV cells, 774 RV cells from 3 mice), PKP2cKO (red bars; n=763 LV cells, 812 RV cells from 3 mice) and PKP2-Cx43-cKO (blue bars;

n=617 LV cells, 729 RV cells from 2 mice). Statistical test: Two-way repeated measures analysis of variance (ANOVA)-Bonferroni ***p<0.001 vs. control; $^{\dagger\dagger\dagger}p$<0.001 vs. LV; $^{\#\#\#}p$<0.001 vs. PKP2cKO. **C**: Mean of the calculated values of $[Ca^{2+}]_i$ after calibration of intensity ratios (see "Methods" for details). Control: n=34 LV cells, 32 RV cells from 4 mice. PKP2cKO n=29 LV cells, 28 RV cells from 4 mice. PKP2cKO/Cx43+/− refers to a PKP2cKO mice also heterozygous-null for Cx43 in cardiomyocytes (see also Methods). n=21 LV cells, 23 RV cells from 3 mice. Statistical test: Hierarchical analysis. *p<0.05 vs. control; $^{\#}p$<0.05 vs. PKP2cKO. **D**: Ca^{2+} spark frequency is significantly dampened by reduced Cx43 expression (green bar). Note that data for RV and LV Ctrl and PKP2cKO is reproduced from previous figures and presented here for comparison against PKP2cKO/Cx43+/−. Hierarchical analysis: PKP2cKOCx43+/−: n=18 LV cells, 21 RV cells from 3 mice. *p<0.05 vs. control; $^{\dagger}p$<0.05 vs. LV; $^{\#}p$<0.05 vs. PKP2cKO.

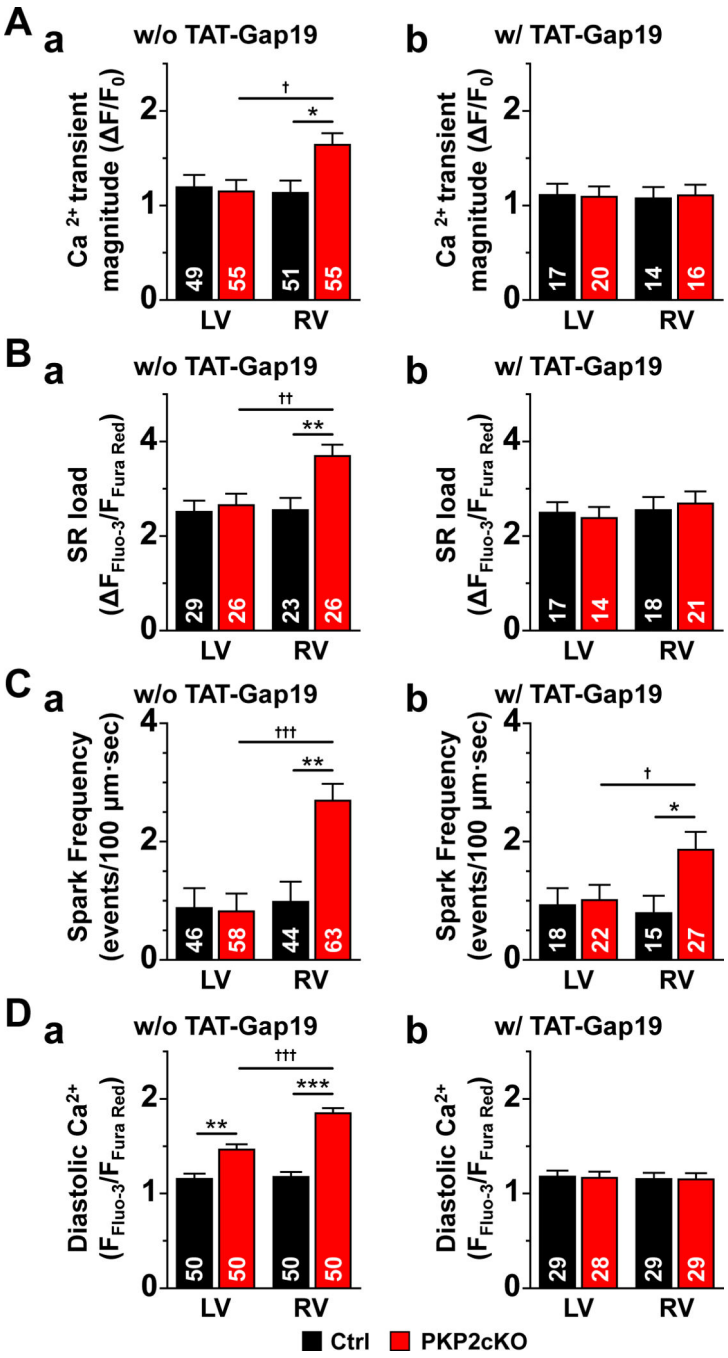

Figure 8. Effect of the Cx43 hemichannel blocker TAT-Gap19 on intracellular calcium homeostasis in PKP2cKO mice.

The left side (panels "**a**") of panels **A**-**D** reproduce data presented in previous figures, for comparison. Transactivator of transcription (TAT)-Gap19 (panels "**b**") normalized the increased Ca^{2+} transient magnitude (relative transient amplitude), sarcoplasmic reticulum (SR) load and elevated diastolic Ca^{2+} and reduced the spark frequency toward values similar to those measured in myocytes of plakophilin-2 conditional knockout (PKP2cKO)-left ventricle (LV) and in controls. Statistical analysis in right panels: Two-way repeated

measures analysis of variance (ANOVA)-Bonferroni for Ca^{2+} transients, SR load and diastolic Ca^{2+}. Hierarchical analysis for Ca^{2+} spark frequency. *p<0.05 vs. control. $^{\dagger}p$<0.05 vs. LV. 3 mice. Numbers in columns indicate number of cells tested.